Available online at www.sciencedirect.com

ScienceDirect

Advances in Space Research xxx (xxxx) xxx

ADVANCES IN SPACE RESEARCH (a COSPAR publication)

www.elsevier.com/locate/asr

Observations and statistical studies of orbit-driven plasma waves in low earth orbit at very low frequencies

Joe Hughes [a,b,*], Ian Collett [b], Camella Nasr [b], Anastasia Newheart [b], Ryan Kelly [b], Scott Thaller [b], Raj Patel [b], Connor Johnstone [b], Elijah Vance [b], Houjun Wang [b], Nathan Re [c], Ben Tatman [c], Yoshiya Kasahara [d], Shoya Matsuda [d], Atsushi Kumamoto [e], Fuminori Tsuchiya [e], Tomoaki Hori [f], Atsuki Shinbori [f], Ayako Matsuoka [g], Mariko Teramoto [h], Kazuhiro Yamamoto [f], Yoshizumi Miyoshi [f], Iku Shinohara [i]

[a] *Northwest Research Associates, 3380 Mitchell Ln, Boulder 80301, USA*
[b] *Orion Space Solutions, 282 Century Pl Suite 1000, Louisville 80027, USA*
[c] *Advanced Space, 1400 W 122nd Ave, Westminster 80234, USA*
[d] *Graduate School of Natural Science and Technology, Kanazawa University, Kakuma, Kanazawa, Ishikawa 920-1192, Japan*
[e] *Tohoku University, Japan*
[f] *Institute for Space-Earth Environmental Research, Nagoya University, Furo-cho, Chikusa 464-8601, Japan*
[g] *Kyoto University, Japan*
[h] *Kyushu Institute for Technology, Japan*
[i] *ISAS/JAXA, Japan*

Received 25 April 2025; received in revised form 25 June 2025; accepted 4 July 2025

Abstract

The number of resident space objects (RSOs), including debris and inactive satellites, is rapidly increasing, posing a growing threat to operational spacecraft. Additionally, many of these RSOs are too small to be reliably tracked by current radars. A novel solution to this problem is to use the disturbances in the plasma environment to track these objects. Over the last decade, theoretical, numerical, laboratory, and observational efforts have studied the generation and propagation of these disturbances.

This study investigates these disturbances statistically using 5 months of Very Low Frequency (VLF) Electric (E) field data collected by the Arase satellite. This represents the first large-scale statistical observational study of RSO-generated waves. Specifically, we use E field power between 1 and 20 kHz from the Onboard Frequency Analyzer, which is part of the Plasma Wave Experiment (PWE) onboard the Arase satellite. We analyze this dataset by comparing the power between an "experiment" population of measurements taken where Arase was in a situation where RSO-generated waves would be observed, and a "control" population where Arase was in a situation where no RSO-generated waves would be observed. For robust comparisons, the two populations should have similar distributions of latitude, longitude, altitude, and time. However, rigidly enforcing this matching results in very small sample sizes. We therefore use three different approaches to this balancing. Our strongest results have a *p*-value of 1.3e-5, indicating that there is a less than 1 in 77,000 chance that the experiment and control populations are drawn from the same parent population. We take this as strong statistical evidence of RSO-generated waves. These encouraging results bolster the feasibility of using these waves as part of a future detection, identification, and tracking system.

Keywords: Space debris; Plasma wave; VLF

* Corresponding author at: Northwest Research Associates, 3380 Mitchell Ln, Boulder 80301, USA.
E-mail address: jhughes@nwra.com (J. Hughes)

https://doi.org/10.1016/j.asr.2025.07.013
0273-1177/

1. Introduction

The IARPA SINTRA (Space object IdeNtification and TRAcking) program aims to drive the state of the art in detecting, tracking, and characterizing space debris. The program seeks to detect debris as small as 1 mm in LEO (Low Earth Orbit) and as small as 1 cm in GEO (Geosynchronous Earth Orbit). Detecting and tracking small debris is vital to our space-faring society, because even a small ~1 g piece of debris can cause mission-ending damage to operational satellites.

As of May 2024, Space-Track.org monitors approximately ~45,000 objects in orbit. When supplemented with model-based estimates for small, untracked objects, this number rises dramatically. Using ESA's MASTER-8 program (Braun et al., 2021) yields estimates of 1.2 Million objects between 1 cm and 10 cm, and 140 million objects between 1 mm and 1 cm. [1] These small debris objects are difficult to reliably detect and track with conventional means. It has been hypothesized that this hard-to-track population of debris might be easier to track by measuring disturbances in the ionosphere and linking them to the nearby objects (Sen et al., 2015a; Truitt and Hartzell, 2020a; Truitt and Hartzell, 2020b). To use an analogy: a small boat on a calm lake may be more easily identified by the wake it leaves behind than by direct observation.

Disturbances to the ambient plasma environment caused by spacecraft belong to a fairly new field of investigation. Throughout this paper, we sometimes refer to these spacecraft as "generators", positing that they generate electrostatic and/or electromagnetic waves. Most of this effort has taken place over the last ~10 years and has approached the problem primarily from the standpoint of theory and simulation. These efforts have identified that soliton waves could be emitted by charged generators. Solitons are nonlinear and nondispersive waves that travel as solitary pulses in the electric field, magnetic field, or electron density, with a monopolar or bipolar structure. Solitons are often studied theoretically in the context of solutions to nonlinear wave equations such as the Korteweg–de Vries, nonlinear Schrödinger, and Kadomtsev–Petviashvili equations (Sen et al., 2015b).

The excitation and propagation of these waves from charged orbiting objects have been studied both theoretically (Acharya et al., 2021a; Acharya et al., 2021b; Acharya et al., 2022; Acharya et al., 2024; Mukherjee et al., 2021) and in numerical simulations (Sen et al., 2015b; Sen et al., 2023). Solitons can manifest in the context of various plasma wave types. A subset of solitons causes electron density perturbations, which may be observable with remote sensing techniques, such as ion acoustic solitons and magnetosonic solitons (Sen et al., 2023). These solitons may remain 'pinned' to the source object or propagate upstream of the generator, potentially serving as an early-warning signal for impending collisions. Several numerical simulation studies have been conducted and suggest that the formation of these solitons should occur (Acharya et al., 2021a; Sen et al., 2015b; Tiwari and Sen, 2016a; Tiwari and Sen, 2016b; Dharodi et al., 2023; Truitt and Hartzell, 2020d; Truitt and Hartzell, 2020c; Truitt and Hartzell, 2021; Resendiz Lira et al., 2024; Ganguli et al., 2025). Laboratory experiments have also shown soliton formation under conditions similar to a charged RSO moving through LEO plasma (Jaiswal et al., 2016).

In observational studies, orbit-driven waves have been studied using the e-POP instrument suite on the Swarm-E/CASSIOPE satellite, which was designed to study geomagnetic storms and ion outflow. e-POP's Radio Receiver Instrument (RRI) observed short, intense amplifications of the electric (E) field wave spectra from 1–5 kHz when e-POP passed near another spacecraft. Detections were observed four times: twice with a Starlink satellite (20 km and 1.17 km closest approach), once with an Iridium Satellite (7.2 km), and once with a piece of Cosmos debris (6.3 km) (Bernhardt et al., 2023 and Eliasson and Bernhardt, 2025). None of these generators were thrusting near the time of conjunction, ruling out propulsion-related wave generation as a cause (e.g. (Bernhardt et al., 2021)). The authors conclude that these are likely compressional Alfvén and weak whistler mode waves.

Our study builds on these prior theoretical, numerical, experimental, and observational studies. We use electric field spectra from 1 to 20 kHz collected by JAXA's Arase satellite to investigate whether RSOs can measurably influence the plasma wave environment in LEO. We show case studies, and for the first time, we present statistical analyses of the influence of RSOs on the plasma wave environment in LEO.

This paper is organized as follows: Section 2 discusses the data and curation methods. Section 3 presents an intriguing case study that motivates five hypotheses to test. Section 4 discusses the statistical methods that are used to test these hypotheses. Section 5 presents the results of our statistical test and verdicts on the five hypotheses. Finally, we summarize and conclude in Section 6.

2. Data and curation process

Arase is a scientific satellite primarily designed to study the Van Allen belts (Miyoshi et al., 2018). Among other science payloads, it carries the Plasma Wave Experiment (PWE), with E and B field probes (Kasahara et al., 2018). The Onboard Frequency Analyzer (OFA) (Matsuda et al., 2018), one of several PWE systems, provides E and B field measurements up to 20 kHz every 8 s. Arase is in a highly elliptical orbit with an apogee altitude of ~32,000 km and a perigee altitude of ~440 km. In each orbit (9.4-h period), Arase spends about 15 min below an altitude of 1,000 km at latitudes between 0 and

[1] https://www.esa.int/Space_Safety/Space_Debris/Space_debris_by_the_numbers?

+ 31 degrees. These "perigee passes" serve as opportunities to study the influence of RSOs on the plasma wave environment in LEO.

We process 5 months of perigee passes (April to September 2018). Our curated dataset includes orbital information, plasma wave measurements, and 'ancillary' contextual environmental data for each pass. The dataset, summarized in Table 1, contains information about nearby generators, Arase data, and ancillary data. To obtain generator information, we propagate orbits using the Two Line Element sets (TLEs) for every object in the Space-Track database. Generator positions and velocities are recorded whenever an object comes within 500 km of Arase. Additionally, the name and Radar Cross Section (RCS) of each generator are retrieved from CelesTrak.

For Arase, we use the definitive orbit data for position and the electron density data derived from the PWE-HFA (Kumamoto et al., 2018) and MGF (Matsuoka et al., 2018). Electric and magnetic field spectrograms are obtained from the PWE/OFA Level 3 wave property data (Kasahara et al., 2021). Ancillary data consist of model-based estimates of electron density (from the International Reference Ionosphere model, IRI) and Earth's magnetic field (from the International Geomagnetic Reference Field model, IGRF) at the location of Arase. The structure and sources of all variables are summarized in Table 1.

In total, this 5-month dataset includes 311 Arase perigee passes, 289 of which pass all quality checks. During this time, Arase comes within 500 km of over 8,000 unique generators. The 25 %, 50 %, and 75 % percentiles of the RCS for all of these encounters are 0.0112, 0.0198, and 0.1532 m^2, respectively. Using the square root of the RCS as a proxy for size, the median debris measures 14 cm in size, and more than 75 % measure less than 40 cm.

3. Hypothesis generation

As a motivating example, Fig. 1 shows the generator information and Arase observations for a single perigee pass on 2018/05/06, starting at 15:49 UT. The top panel shows the distance between Arase and the various generators it encounters during the perigee pass. The line for each generator is color-coded by size. Table 2 provides more information on the five generators that pass within 100 km of Arase. The bottom two panels of Fig. 1 show the E and B field total wave power spectrograms from the Arase PWE/OFA L3 wave property data. Several plasma lines of interest (plasma, gyro, and lower hybrid frequencies for O + and H+) are overlaid. Plasma lines are computed using magnetic field strength from the IGRF model and electron density from either the IRI model (lines) or Arase density data (points). The IRI densities are especially useful at lower altitudes, where the PWE/HFA-derived densities are too high for reliable measurement. The latitude, longitude, and altitude of Arase every 2 min are written under the axis for spatial context.

Two enhancements in E field power appear near when Generator 2 (Cosmos 1892) reaches its point of closest approach with Arase (16.6 km). The higher-frequency of the two is ~18 kHz, which is near the hydrogen lower hybrid frequency for this location. The second is more broad band, spread between 2–10 kHz, which could be an oxygen lower hybrid wave.

However, a skeptic could easily argue that this enhancement was caused by a unrelated process such as a lightning-generated whistler or ground-based VLF transmitter and Cosmos 1892 just happened to be nearby when it occurred. There are also many close approaches that do not lead to enhancements. To robustly test the existence of RSO-generated waves, we use statistical techniques to compare the E field power when we would expect Arase to measure them to the power when we do not expect Arase to measure these waves. To quantify when we ought to expect to measure waves, we present five wave generation mechanisms.

3.1. Wave generation mechanisms

Based on systematic review of many perigee passes such as the one shown in Fig. 1, we define five testable hypotheses that predict when Arase should observe enhanced E field power due to nearby RSOs. In cases with clear enhancements, B field signatures are usually absent; we therefore focus on the E field throughout the remainder of this study.

Two conditions must be satisfied for Arase to detect an RSO-generated wave: (1) the wave must actually be launched by the generator, and (2) Arase must be positioned to observe it. The first condition may depend on the generator's charge state, direction of motion relative to the magnetic field, or the local plasma environment. In

Table 1
Organization of the data into different categories.

Category	Variable	Source
Nearby Generators	NORAD ID, Name, Radar Cross Section	CelesTrak
	Position and Velocity	Space-Track.org
Arase	Position	Arase L2 definitive orbit data
	E and B field Spectrograms	Arase PWE/OFA L3 wave property data
	Electron Density	Arase PWE/HFA L3 electron density data
Ancillary	Electron Density	International Reference Ionosphere (IRI)
	Magnetic Field	International Geomagnetic Reference Field (IGRF-13)

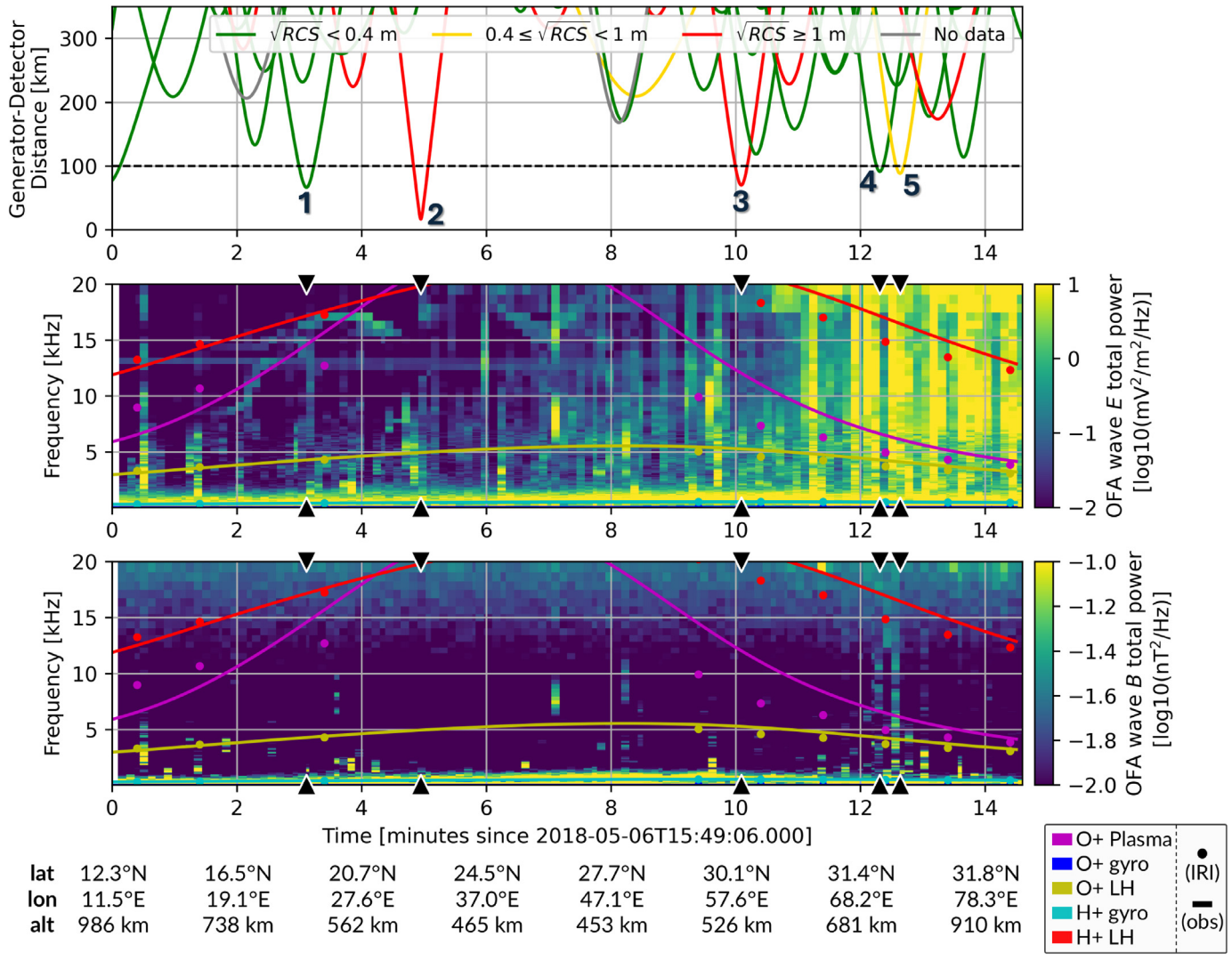

Fig. 1. Arase measurements and generator information for a single perigee pass. (top) Distance between Arase and each generator, with color as a proxy for generator size. (middle) Electric field measurements from Arase. (bottom) Magnetic field measurements from Arase. In this panel, colored lines show model estimates of relevant frequencies while points of the same color show observed frequencies from the Arase density data. The purple line represents IRI O + plasma frequency, blue is for O + gyro frequency, cyan is for H + gyrofrequency, yellow is for O + lower hybrid, and red is for H + lower hybrid.

Table 2
Information for the 5 near-approaching generators noted in Fig. 1. 'DEB' in the name indicates a debris object.

	Name	Size (m)	dx (km)
1	CZ-4B DEB	0.21	66.4
2	COSMOS 1892	2.53	16.6
3	ERS-2	3.09	69.9
4	FENGYUNG 1C DEB	0.09	91.3
5	NOAA 11 DEB	0.53	88.3

this study, we assume all generators emit waves continuously and instead focus solely on the second condition—whether Arase is geometrically well-positioned to detect those waves. Theoretical analysis by (Bernhardt et al., 2023; Eliasson and Bernhardt, 2025; Resendiz Lira et al., 2024; Ganguli et al., 2025), has shown that the expected wave types generated by RSOs are lower hybrid, fast mode Alfven, and whistler waves which propagate perpendicular to B, isotopically, and within ~19.5 degrees of B. This motivates three primary geometric hypotheses, each shown in Fig. 2. In this schematic, blue arrows indicate the direction of motion of either the generator (gold circle labeled 'G') or detector (shown with an image of the Arase satellite). Each hypothesis defines a scalar score over time that we use in the statistical analysis in Sections 4 and 5.

3.1.1. Hypothesis 1: dx

The simplest and first hypothesis is that there is an increase in the E field power whenever the detector is near a generator. This assumes that waves propagate isotropically. To quantify this, let Δx be the distance between Arase and each generator in kilometers. Δx is of shape $[N_T, N_G]$ where N_T is the total number of measurements in our data-

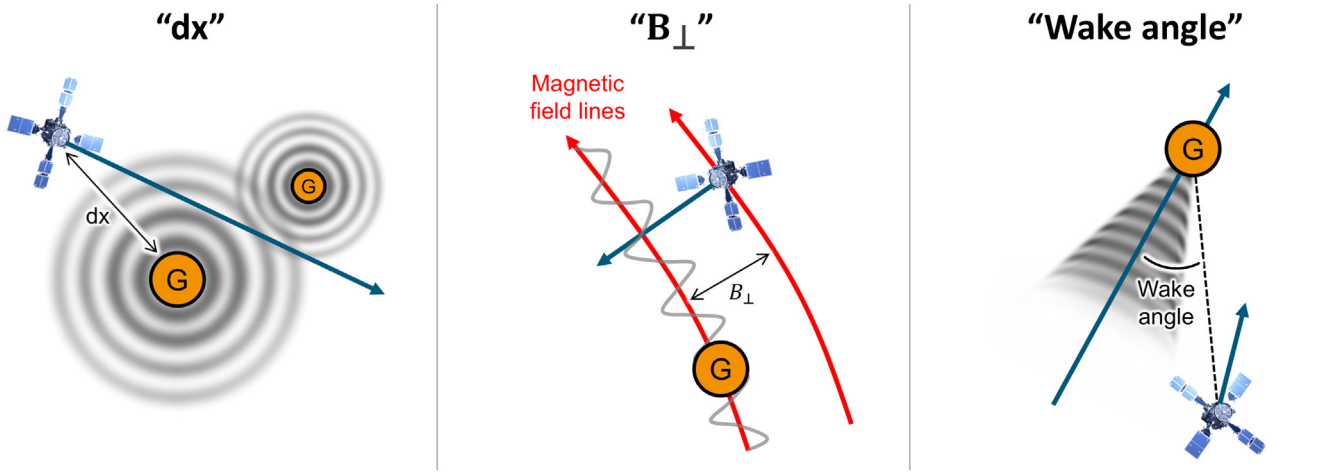

Fig. 2. Three primary hypotheses for orbit-driven wave generation. (left) The "dx" hypothesis postulates that Arase measures higher power when it is close to a generator. (middle) The "$B_\perp$" hypothesis postulates that Arase measures more power when it is on the same magnetic field line as a generator. (right) The "wake angle" hypothesis postulates that Arase measures more power when it is behind a generator.

set and N_G is the total number of unique generators. Our score for this hypothesis is given by:

$$s = \text{Minimum}_G(\vec{\Delta x}) \tag{1}$$

where $\text{Minimum}_{G()}$ indicates the minimum across the last axis of the value inside the parentheses. This score is now only a function of time, and can be visualized as the lower boundary of all the Generator-Detector distances shown in the upper panel of Fig. 1. If this hypothesis is correct, then Arase will measure more E field power when close to a generator.

3.1.2. Hypothesis 2: $B_\perp$

The second hypothesis is that Arase measures an increase in E field power whenever it is on the same B field line as a generator. "$B_\perp$" refers to the distance between the magnetic field line that passes through the generator and the magnetic field line that passes through Arase, each shown as a curved red arrow in Fig. 2. The distance is labeled as $B_\perp$ in the illustration. This hypothesis assumes that waves travel preferentially along magnetic field lines. To quantify this, let $\vec{B_\perp}$ denote the distance across field lines for each generator in kilometers. Like Δx, this variable is of shape $[N_T, N_G]$. Our score for this hypothesis is given by:

$$s = \text{Minimum}_G(\vec{B_\perp}) \tag{2}$$

where $\text{Minimum}_{G()}$ again indicates the minimum across the last axis of the value inside the parentheses so that the score is only a function of time. If this hypothesis is correct, then Arase will measure more E field power when directly north or south of a generator. Since our dataset only contains generators within 500 km of Arase, this score does not consider generators on the same field line but half a hemisphere away.

3.1.3. Hypothesis 3: wake angle

The third hypothesis assumes that the waves propagate as a bow wave and will be found in the wake of the generator. Spacecraft-generated waves have been observed in the wake of a spacecraft in the solar wind plasma (Malaspina et al., 2022), and a similar thing may happen in LEO. To quantify this, let $\vec{\theta}$ denote the wake angle to each generator. θ is 0^o when Arase is in the generator aft direction, and 180^o when Arase is in the generator ram direction. As with $\vec{B_\perp}$ and $\vec{\Delta x}, \vec{\theta}$ is of shape $[N_T, N_G]$. Our score for this hypothesis is given by:

$$s = \text{Minimum}_G(\vec{\theta}) \tag{3}$$

where $\text{Minimum}_{G()}$, once again, indicates the minimum across all generators. Since our dataset only contains generators within 500 km of Arase, this score does not consider generators directly infront of Arase but half an orbit away. If this hypothesis is true, Arase will measure more E field power when just behind a generator.

3.1.4. Hypothesis 4: cumulative free-space power

Hypotheses 4 and 5 are variants of Hypothesis 1, but accumulate effects from all generators instead of just one. Hypothesis 4 first forms the total power, and then inverts it to make the score. The power from each generator is proportional to its cross sectional area, and inversely proportional to the square of the distance to Arase. Power should follow an inverse square law in free space, which explains the name of this hypothesis. The total power is the sum of the power from each generator:

$$P_T = \sum_G \frac{\text{RCS}}{dx^2}, \qquad s = \frac{1}{P_T} \tag{4}$$

where $\sum_G$ denotes a sum over all generators. To calculate the score, we take the inverse of total power.

3.1.5. Hypothesis 5: cumulative plasma power

This hypothesis is very similar to Hypothesis 4, but it assumes the power from each generator is proportional to the product of the cross-sectional area and an exponential decay function of distance. This form is expected for waves decaying in a plasma, which explains the name of this hypothesis. The total power is the sum of the power from each generator:

$$P_T = \sum_G \mathrm{RCS} e^{\frac{-dx}{\lambda}}, \qquad s = \frac{1}{P_T} \tag{5}$$

where $\sum_G$ again denotes a sum over all generators, and λ is the scale length. A value of 100 km is used for λ in this study. This value was chosen somewhat arbitrarily to be within the range of generator distances and separate this hypothesis from the prior one.

4. Statistical methods

These five wave generation mechanisms are used to determine when we would expect Arase to measure more power due to generator-driven waves. To test our hypotheses robustly, we developed a three-step process that is conceptually represented in Fig. 3.

1. Define a numerical score related to the hypothesis. The score is a scalar function of time. A low score indicates that Arase is in a scenario in which we hypothesize a disturbance would be measured. A high numerical score indicates that Arase is not in that scenario. The score for each hypothesis is described in the previous section.
2. Select "experiment" and "control" populations from the 5-month dataset. The experiment contains Arase observations from times when the score was low, and the control contains Arase observations from times when the score was high. In Fig. 3, measurements made at t_2 and t_3 go into the experiment population, whereas t_5 goes into control. Measurements made at t_1 and t_4 are not used.
3. Compare distributions of the E field power between the control and experiment populations. If they are statistically different, and differences between the populations unrelated to generator effects have been sufficiently mitigated, we consider this evidence of generator signatures consistent with the hypothesis being tested.

The two histograms in the right panel of Fig. 3 provide an illustrative example of Step 3. The distribution of power in the experiment population (green) is higher than the distribution of power in the control population (red).

As previously stated, a statistically significant difference between the experiment and control populations should only be considered as evidence of generator effects if other differences between the populations are minimized to the degree possible. To discuss this more easily, we will define the term "latent variable" to mean a variable that could cause a change in the Arase measurements and correlate with variables that contribute to the score in one of our hypotheses. For example, Arase measures higher VLF wave power in certain longitudinal sectors due to lightning sferics and terrestrial VLF transmitters (e.g. (Colman and Starks, 2013; Cohen et al., 2012)). If the experiment population happens to contain more observations from these sectors than the control population, then it would be hard to argue that larger power values in the experiment population are due to orbit-driven wave effects rather than lightning or sferics. In this example, longitude is a latent variable. Other relevant latent variables include, but are not limited to, latitude, local time, altitude, season, and

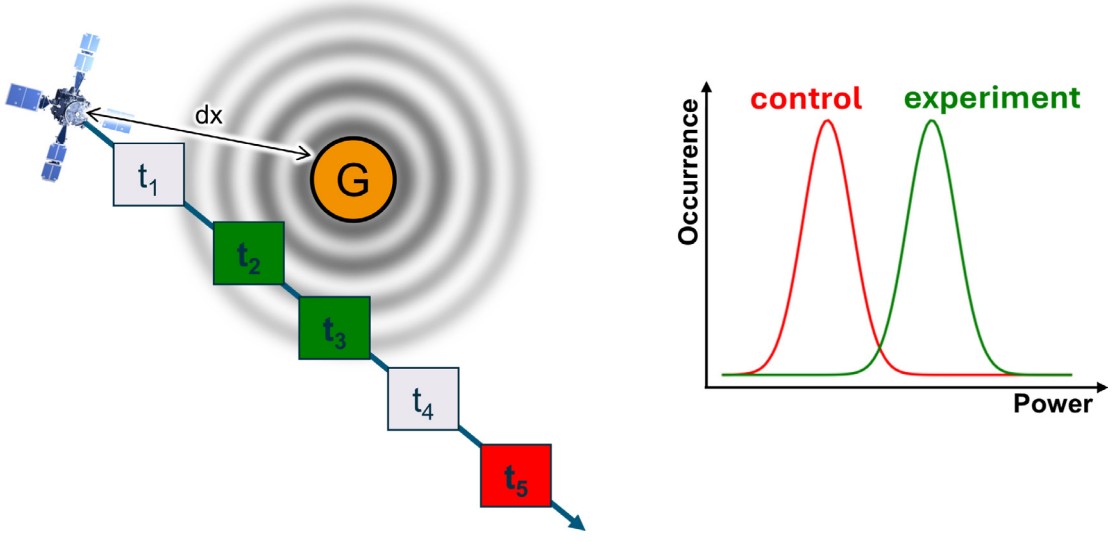

Fig. 3. Concept for selecting experiment and control populations. (left) The "dx" hypothesis postulates that more power is measured when Arase is close to a generator, so measurements made at t_2 and t_3 are added to the experiment population, whereas the measurement made at t_5 goes into control. Measurements made at t_1 and t_4 are not used. (right) Conceptual histogram of the power in the experiment and control populations.

geophysical activity. To minimize differences between the populations, we balance the populations across latent variables. However, balancing the experiment and control populations across many latent variables reduces the total size of both populations which decreases the statistical confidence level. We have developed a way to pick both populations in a way that maximizes the score difference while balancing the latent variables to the degree possible.

4.1. Population picking

When choosing the experiment and control distributions from our 5-month sample set of observations from Arase, our goal was to minimize the score of the experiment distribution and to maximize the score of the control population, while diminishing the effects of latent variables. We developed an algorithm to simultaneously balance the two distributions over their latent variables, while maximizing the difference in their average score. The algorithm additionally allows for the specification of a maximum score for the experiment population and a minimum score for the control population as preliminary filters.

To compute the two distributions, we first provide a list of values for each latent variable, which act as bins to create a n-dimensional grid-based partition of the full sample distribution, where n is the number of latent variables. For example, when using longitude and local time as latent variables, we might provide the longitudes [-90, −30, 30, 90] (in degrees) and local times [0, 12, 24] (in hours), which results in a 3 by 2 grid that partitions the two-dimensional latent space into six bins. In this example, the first bin consists of samples for which the Arase satellite is between −90 and −30 degrees latitude and between 0 and 12 h in local time. Within each bin, we first sort the samples based on their score, then we iteratively pair the samples at either end of the list–maximizing the difference in score between pairs–and remove the two samples after they have been paired. During this process, we record the difference in score between the pairs. Once we have no more samples within a bin that fall inside our predefined score cutoffs, we move onto the next bin. After accumulating these pairs of samples for all bins, we sort the pairs based on their difference in score, and select the (at most) N pairs that have the largest difference in score, where N is a predefined number of maximum samples. This population picking algorithm ensures that the chosen experiment and control distributions have the same number of samples, balances over their latent variables, and maximizes the difference in average score of the two distributions while enforcing predefined distribution score cutoffs.

In practice, we want to minimize the effect that the latent variables can have on our hypothesis, thereby minimizing the size of each bin. However, by minimizing the size of each bin we reduce the number of samples in each bin, and thus limit the number of potential pairs we can form between samples. This limits the size of the experiment and control populations. If there are too few samples in the two distributions, then any hypothesis about the effect of the chosen score might have on the E field power measured by Arase is less statistically valid. Hence, when choosing bin sizes for the latent variables a balance must be struck between minimizing the bin sizes and maximizing the number of samples in each bin.

5. Results

Fig. 4 summarizes the statistical analysis for the proximity hypothesis. Fig. 4(d) shows the distribution of the score (distance to the closest generator, in this case) for both populations and the total population. Cutoffs were enforced for both populations—the experiment can only contain samples with a score below 150 km, and the control can only contain samples with scores above 300 km. These populations were chosen using latent variables of altitude (30 bins) and file index. Since each perigee pass covers a small geographical area, enforcing strict file matching indirectly enforces latitude and longitude matching as well. This resulted in a sample size of 709 for both the experiment and control.

Figs. 4(a) and 4(b) show histograms of the E field power across all spectral frequencies for the experiment and control populations. Fig. 4(c) shows the counts in the experiment histograms divided by the counts in the control histogram. Red colors (ratio > 1) above the dashed black median line and blue colors (ratio < 1) below indicate that the experiment population tends to have higher power values than the control population at that frequency, implying that generators produce waves. This trend appears to be strongest above 5 kHz.

Similarly, Fig. 5 provides the results of the $B_{\perp}$ hypothesis, where the score is the nearest distance to a generator across field lines. The distributions of the score for the total, experiment, and control populations are shown in panel (d). The same latent variables (altitude, file index) were used, as well as cutoffs of 100 and 250 km. This results in a population size of 1197 members for each population. Panels (a) and (b) show the counts for each population as a function of power and frequency. Panel (c) shows the ratio of the counts for the experiment and control. This panel shows a strong red region above the black dashed line from ~1–4 kHz and a corresponding blue region below the black dashed median line. This indicates higher power in the experiment population than the control in this frequency range. Hypotheses 3, 4, and 5 are tested in the same manner but do not have as clear differences between the experiment and control. These figures are not included in the main article for brevity.

To further quantify the statistical significance of this result, we applied a one-sided two-sample Kolmogorov–Smirnov (KS) test. This test is similar to Student's t test, but does not assume a normal distribution. Small p values indicate that the experiment is drawn from a distribution that has larger power values than control. The result of the KS test for the "dx" hypothesis is applied at each fre-

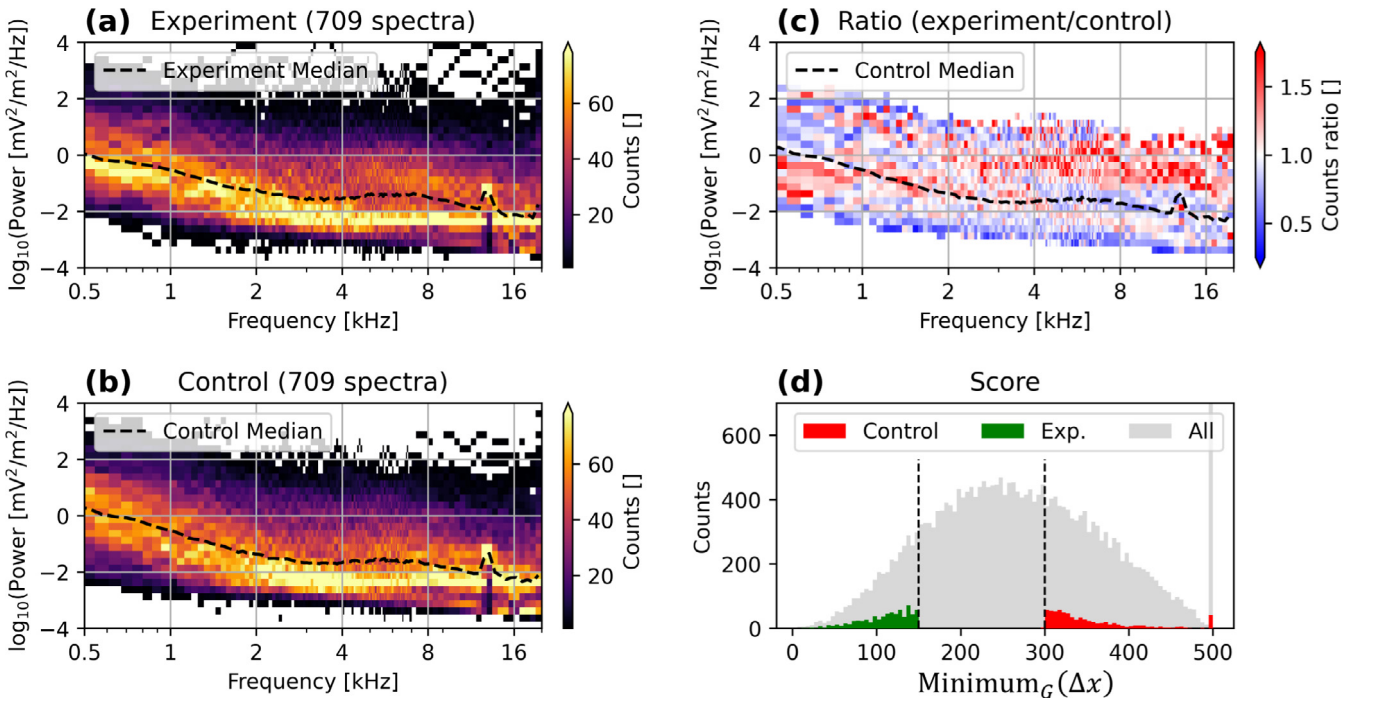

Fig. 4. Statistical results for the "dx" hypothesis. (a) 2D histogram showing the distribution of E field power across frequency for the experiment population. (b) Distribution of E field power across frequency for the control population. (c) The ratio of values in panel (a) to values in panel (b). Red colors indicate a power/frequency combination is more common in the experiment than in the control population. (d) Distribution of the total (grey), experiment (green), and control (red) scores. (For interpretation of the references to colour in this figure legend, the reader is referred to the web version of this article.)

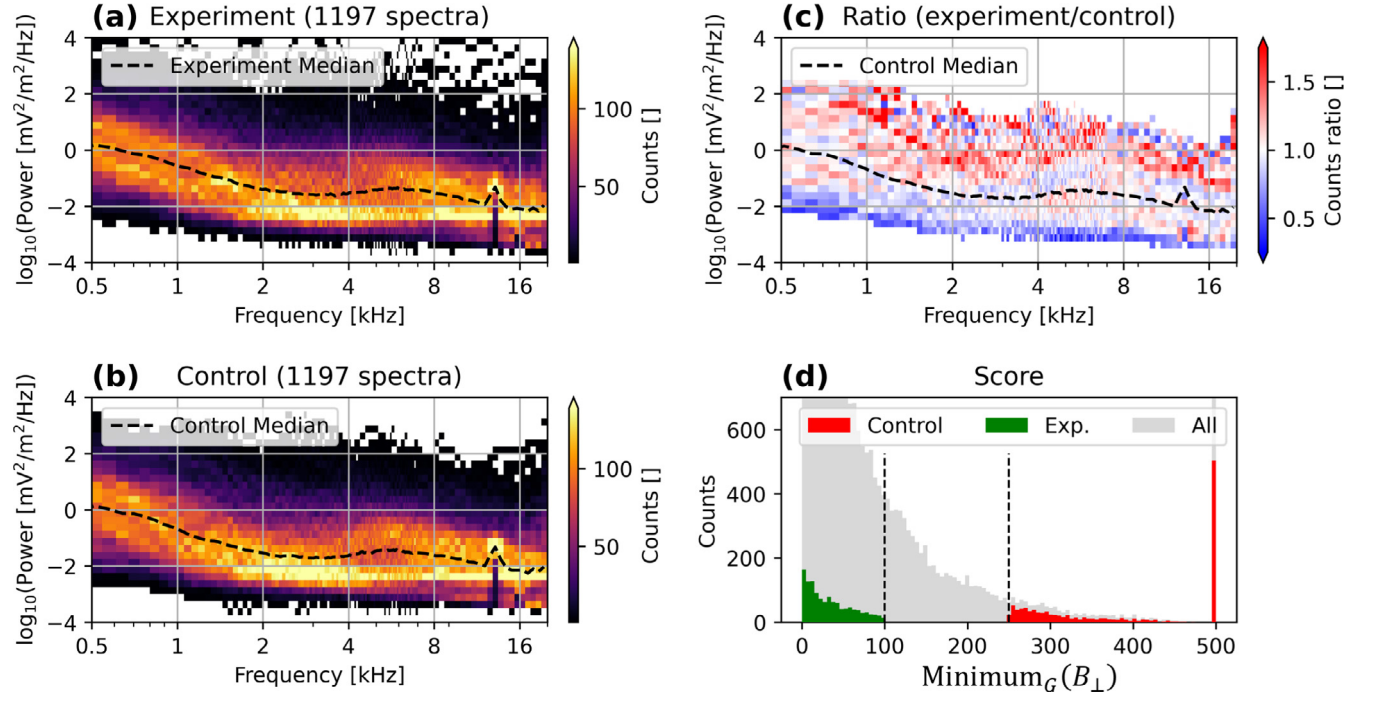

Fig. 5. Statistical results for the "$B_\perp$" hypothesis. Panels are set up correspondingly to Fig. 4.

quency and shown as the blue curve in Fig. 6. For some frequencies above 7 kHz, we see statistically significant evidence that the experiment has higher power values than the control. These results are consistent with generators producing waves in the >7 kHz ranges that propagate isotropically. One hundred random scores are chosen as

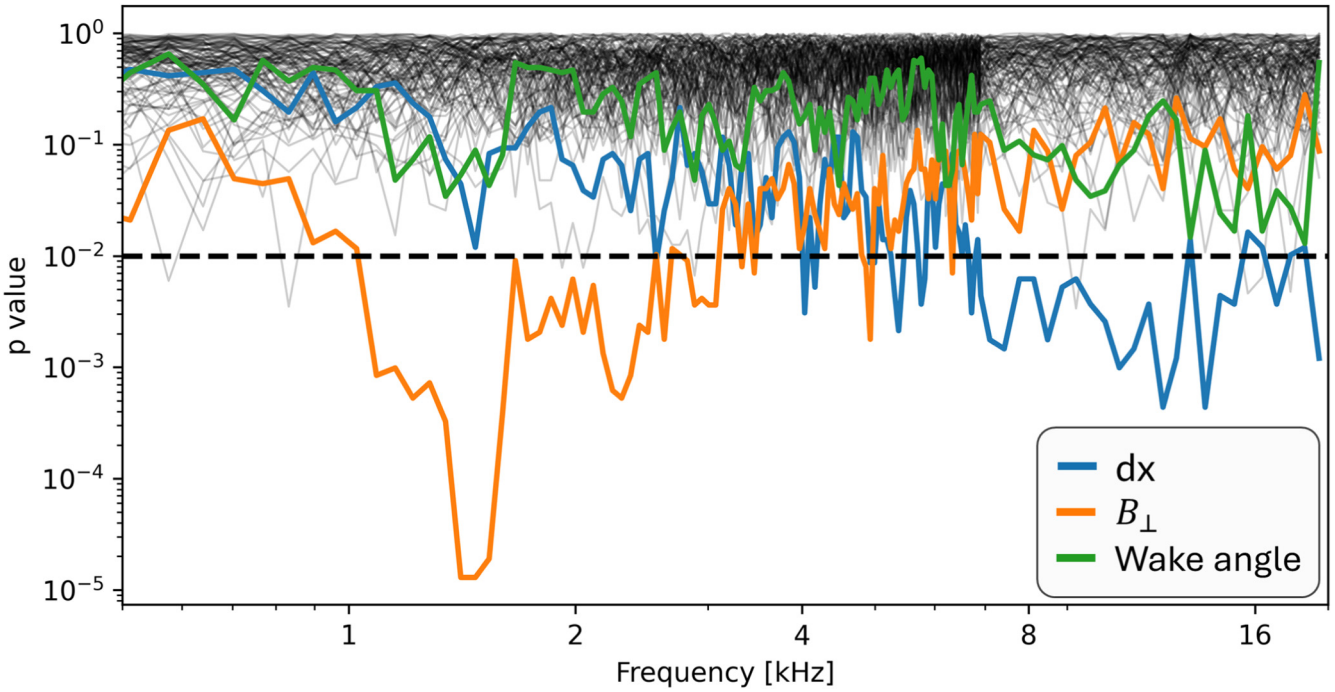

Fig. 6. Probability of the null hypothesis for all three primary hypotheses shown as color. 100 random scores are also chosen and shown as thin black lines to show the natural spread of the data.

an additional point of comparison and the resulting KS tests are shown as the faint black lines in Fig. 6. The fact that none of these tests reach the same level of significance as the proximity hypothesis supports the notion that Arase is observing generator-driven waves and not random effects.

The orange and green lines in Fig. 6 represent the results of the KS tests for the "$B_\perp$" hypothesis (orange) and the "wake angle" hypothesis (green). Results from the "$B_\perp$" hypothesis are consistent with generators producing waves in the 1–4 kHz range that propagate approximately along field lines. For the "wake angle" hypothesis, there are fewer significant signatures, with the *p*-value barely dropping below 0.01. One possibility for the relatively weaker signal for this hypothesis is that the waves produced by this mechanism are ion acoustic waves, which tend to be strongly damped within a wavelength (less than 1 m) unless the plasma electron temperature is significantly larger than that of the ions. This means that ion acoustic waves may indeed be generated, and the "wake angle" hypothesis may be true, but we cannot confirm it using this set of the Arase data.

There are several kinds of waves that could be responsible for the more significant results of our other two hypotheses. Of the kHz frequency waves proposed to be generated by moving space objects (Bernhardt et al., 2023), likely candidates are whistler-mode and lower hybrid waves. The results of our statistical study are consistent with these types of waves. Alfven waves have also been suggested as a wave type generated by moving RSOs but would be at frequencies less than the ion cyclotron frequency (~450 Hz for H + and ~28 Hz for O+). Alfven frequencies are thus below those for which the proximity or "$B_\perp$" hypotheses hold.

5.1. Varying latent variables

The above analysis is for three of our five hypotheses under one set of latent variables. As previously discussed, there are many ways to trade sample size for latent variable matching. To better understand this trade space, we test all five hypotheses under two additional sets of latent variables:

1. Latitude (10 bins), longitude (50 bins), and local time (20 bins). This was done to directly account for location-dependent power from lightning and VLF transmitters (Colman and Starks, 2013; Cohen et al., 2012). Unlike the first latent variable set, this set does not enforce seasonal matching, so a measurement in the experiment population in April could be balanced by a measurement made in the same place and local time, but in September.
2. Latitude (10 bins), longitude (50 bins), local time (20 bins), file index (20 bins). This is the strictest latent variable matching, and accounts for both location, diurnal, and seasonal effects. However, it results in the smallest sample sizes.

The results for all five hypotheses under each of the three sets of latent variables are shown in Table 3. Each row shows the experiment and control size, minimum

Table 3
Population statistics and minimum p values for all five hypotheses and three sets of latent variables.

	Hypothesis	**Latent Variables** [number of bins]	**Size of Exp. and Con.**	**Exp.** s_{max}	**Con.** s_{min}	p_{min}
1	dx [km]	altitude [30], file index [289]	709	150	300	0.000438
2	$B_\perp$ [km]		1197	100	250	1.3e-5
3	wake angle [deg]		1033	40	90	0.013
4	free-space power		381	1.43e + 04	1.45e + 06	0.00618
5	plasma power		374	3.74	411	0.0378
6	dx	latitude [10], longitude [50], local time [20]	1429	150	300	0.0141
7	$B_\perp$		1421	100	250	0.0386
8	wake angle		1500	40	90	0.00572
9	free-space power		671	1.43e + 04	1.45e + 06	0.0817
10	plasma power		660	3.74	411	0.126
11	dx	latitude [10], longitude [50], local time [20], file index [20]	615	150	300	0.0429
12	$B_\perp$		921	100	250	0.0738
13	wake angle		871	40	90	0.174
14	free-space power		204	1.43e + 04	1.45e + 06	0.115
15	plasma power		196	3.74	411	0.192

and maximum scores, and the minimum p-value across all frequencies for a hypothesis and set of latent variables. In the latent variable column, the number in brackets indicates how many bins were used to discretize that variable for balancing. Hypothesis/latent variable combinations that lead to p values below 0.01 (1 in 100 chance of the result being produced by noise) are shaded in light green. The first five rows show the results using the first set of latent variables, three of which are also shown in Figs. 4–6. The next five rows show the results using latitude, longitude, and local time, and the last five rows show the results additionally enforcing file index matching.

The results shown in in Table 3 show that the p-value varies significantly depending on the hypothesis and set of latent variables used for matching. This indicates that spatio-temporal correlated power is significant compared to generator effects. The p-value varies between 1.3e-5 and 0.192, indicating that the probability that the experiment is drawn from the same population as the control is between 1 in ~77,000 and 1 in ~5. As conglomerates, the first set of latent variables leads to lower p-values than the other two. The first set of latent variables lead to three hypotheses passing the arbitrary cutoff of $p = 0.01$. Only one hypothesis (wake angle) passes this cutoff for the other sets of latent variables. The first set of latent variables is unique in strict file matching. The third set uses only 20 bins for discretizing the file index, which translates to a time scale of ~6 days rather than the time scale of ~15 min for the first set. From this, one could conclude that changes in the background at timescales between 15 min and 6 days must be mitigated against for generator effects to appear. Geomagnetic forcing occurs on such timescales, and could be a possible contributor to this variable background.

Although we did not explicitly balance over the RCS of generators, we note that the distribution of sizes for all 15 permutations of hypotheses and latent variables very closely resembles that of the total population. The 25 % and 50 % quantiles are very close to that of the total population with effective sizes of 10.5 and 14 cm. This is less than a 0.2 % change from the total population. The 75 % quantile varies from 0.148 to 0.174 m^2 (38.5 to 41.7 cm) depending on the permutation. This means that our results pertain most strongly to 10–40 cm RSOs.

6. Summary and conclusions

The accumulation of non-maneuverable RSOs in space, particularly in LEO, is an increasingly urgent issue. This congestion presents a serious hazard to space exploration and other space-based activities and assets. Small debris is especially problematic since it cannot easily be detected by radar. However, one promising avenue for detection is looking for possible plasma wave signatures produced by the RSO, rather than relying on conventional sensing techniques. The detection and identification of these waves could result in new methods for the avoidance of these small, yet certainly not harmless, RSOs. Much of the previous work in this area has been theoretical or simulation-based and has provided compelling evidence for the possibility of RSO detection via plasma waves. There have been relatively few space-based explorations of this concept. One study (Bernhardt et al., 2023) presents clear evidence of enhanced plasma waves detected by the e-POP satellite when in close proximity (2–10 km) to known, non-thrusting, objects.

This study advances the field by statistically testing whether RSOs generate observable plasma wave disturbances in LEO, using rigorous control populations. We conduct a statistical investigation using five months of plasma wave data collected by the Arase satellite during its 15-min ionospheric transits. We use known RSO positions to test whether enhanced wave power is observed during conjunctions, compared to matched control periods

without nearby RSOs. We define "latent variables" as factors that may correlate with wave power but are unrelated to RSOs—such as longitude or local time (LT). We mitigate the effects of these latent variables by selecting control populations with distributions matched to those in the experimental population. In this way, five different hypothetical scenarios related to wave propagation are tested. The three primary hypotheses posit that RSO-generated waves propagate: (1) isotropically; (2) along background magnetic field lines; or (3) in a bow wave-like wake. Two additional hypotheses extend the isotropic case by considering the cumulative effects from all generators rather than only the closest one.

Each of these five hypotheses is tested with three different sets of latent variables, producing 15 separate statistical analyses. For each, we use a Kolmogorov–Smirnov test to compute the probability that the experiment and control populations are drawn from the same parent distribution—the p-value. A low p-value supports the hypothesis that Arase is measuring generator-driven effects rather than random fluctuations. This analysis is performed at each frequency across the measured spectrum.

Depending on the hypothesis and latent variable set, the minimum p-value ranges from about 0.2 down to 1.3×10^{-5}—indicating as low as a 1 in 77,000 chance that results arise from background noise alone. Three of the five hypotheses (dx, $B_{\perp}$, and free-space power) pass an arbitrary p-value threshold of 0.01 for the first latent variable set. Only one passes for the second set (wake angle), and none pass for the third set. This implies that statistically significant results only emerge when background variation is tightly constrained by file matching. The most significant frequencies for the "dx" hypothesis are observed in the 10–20 kHz range, while those for the "$B_{\perp}$" hypothesis are seen from 1–4 kHz. These observations are consistent with the properties of whistler-mode and lower hybrid waves.

The field of orbit-driven waves is young, and there are many exciting avenues for future work. Expanding the dataset would improve statistical confidence and enable stricter latent variable matching. Data from other spacecraft—such as the Van Allen Probes or e-POP—could be used to cross-validate findings. Alternate scoring schemes and latent variable sets could also be explored. Future work may also focus on leveraging magnetic field data to better distinguish wave modes and using remote sensing techniques to observe plasma disturbances in situ.

7. Data access

Science data from the ERG (Arase) satellite were obtained from the ERG Science Center operated by ISAS/JAXA and ISEE/Nagoya University (Miyoshi et al., 2018) (https://ergsc.isee.nagoya-u.ac.jp/index.shtml.en, Miyoshi et al., 2018b(#)). This study utilized Arase L2 definitive orbit data (10.34515/DATA.ERG-12000: https://ergsc.isee.nagoya-u.ac.jp/data/ergsc/satellite/erg/orb/def/), PWE OFA L3 wave property data (10.34515/DATA.ERG-08003: https://ergsc.isee.nagoya-u.ac.jp/data/ergsc/satellite/erg/pwe/ofa/l3/property/), and PWE HFA L3 electron density data (10.34515/DATA.ERG-10001: https://ergsc.isee.nagoya-u.ac.jp/data/ergsc/satellite/erg/pwe/hfa/l3/).

Information on tracked space objects was obtained from Space-Track.org and CelesTrak. The International Reference Ionosphere (via pyIRI,https://pypi.org/project/PyIRI/) and the International Geomagnetic Reference Field (IGRF-13) model were used.

As shown in Table 1, we have created a dataset that combines Arase science data with ancillary information about the background plasma density and magnetic field, as well as information about all nearby generators. We refer to this data internally as "Level 2". To respect Arase's rules regarding data distribution, we have removed the Arase data from our "Level 2" product to make a "Level 1.9" product. This includes the IRI, IGRF, and generator information, and it can be found here: https://zenodo.org/records/14721507. To aid those who desire to replicate our results or expand upon them, we also provide software (https://github.com/joe-hughes26/Arase-Object-Detection-Analysis) that will fetch the Arase scientific data and add it to the provided "Level 1.9" data so that users can create their own "Level 2" data. We also provide software to generate figures in the likeness of Figs. 4 and 5 for user-supplied scores.

Declaration of Competing Interest

The authors declare that they have no known competing financial interests or personal relationships that could have appeared to influence the work reported in this paper.

Acknowledgments

This research is based on work supported in part by the Office of the Director of National Intelligence (ODNI), Intelligence Advanced Research Projects Activity (IARPA), via 2023–23060200005. The views and conclusions contained herein are those of the authors, and should not be interpreted as necessarily representing the official policies, either expressed or implied, of ODNI, IARPA, or the U.S. Government. The U.S. Government is authorized to reproduce and distribute reprints for governmental purposes notwithstanding any copyright annotation therein.

During the preparation of this work, the authors used ChatGPT to assist with typesetting and proofreading. After using this tool/service, the authors reviewed and edited the content as needed and take full responsibility for the content of the publication.

References

Acharya, S.P., Mukherjee, A., Janaki, M.S., 2021a. Accelerated magnetosonic lump wave solutions by orbiting charged space debris. Nonlinear Dyn. 105. https://doi.org/10.1007/s11071-021-06594-x.

Acharya, S.P., Mukherjee, A., Janaki, M.S., 2021b. Bending of pinned dust-ion acoustic solitary waves in presence of charged space debris. Phys. Rev. E 104. https://doi.org/10.1103/PhysRevE.104.014214.

Acharya, S.P., Mukherjee, A., Janaki, M.S., 2022. Charged space debris induced nonlinear magnetosonic waves using inertial magnetohydrodynamics. Adv. Space Res. 69. https://doi.org/10.1016/j.asr.2022.03.020.

Acharya, S.P., Mukherjee, A., Janaki, M.S., 2024. Exact ion acoustic n solitary waves with variable velocity in inhomogeneous plasma induced by charged space debris. Phys. Scr. 99, 55235. https://doi.org/10.1088/1402-4896/ad3997.

Bernhardt, P.A., Bougas, W.C., Griffin, M.K. et al., 2021. Strong amplification of elf/vlf signals in space using neutral gas injections from a satellite rocket engine. Radio Sci., 56(2), e2020RS007207. URL:https://agupubs.onlinelibrary.wiley.com/doi/abs/10.1029/2020RS007207. arXiv:https://agupubs.onlinelibrary.wiley.com/doi/pdf/10.1029/2020RS007207. E2020RS007207 2020RS007207.

Bernhardt, P.A., Scott, L., Howarth, A., et al., 2023. Observations of plasma waves generated by charged space objects. Phys. Plasmas 30. https://doi.org/10.1063/5.0155454.

Braun, V., Horstmann, A., Lemmens, S., et al., 2021. Recent developments in space debris environment modelling, verification and validation with master. In: Proceedings of the 8th European Conference on Space Debris. European Space Agency (ESA), Darmstadt, Germany, URL: https://conference.sdo.esoc.esa.int/proceedings/sdc8/paper/28/SDC8-paper28.pdf.

Cohen, M.B., Lehtinen, N.G., Inan, U.S., 2012. Models of ionospheric vlf absorption of powerful ground based transmitters. Geophys. Res. Lett., 39(24). URL:https://agupubs.onlinelibrary.wiley.com/doi/abs/10.1029/2012GL054437. arXiv:https://agupubs.onlinelibrary.wiley.-com/doi/pdf/10.1029/2012GL054437.

Colman, J.J., & Starks, M.J. (2013). Vlf wave intensity in the plasmasphere due to tropospheric lightning. Journal of Geophysical Research: Space Physics, 118(7), 4471–4482. URL: https://agupubs.onlinelibrary.wiley.com/doi/abs/10.1002/jgra.50217. doi: 10.1002/jgra.50217. arXiv:https://agupubs.onlinelibrary.wiley.com/doi/pdf/10.1002/jgra.50217.

Dharodi, V., Kumar, A., Sen, A., 2023. Signatures of an energetic charged body streaming in a plasma. Phys. Rev. E 107. https://doi.org/10.1103/PhysRevE.107.025207.

Eliasson, B., Bernhardt, P.A., 2025. The generation of whistler, lower hybrid, and magnetosonic waves by satellites passing through ionospheric magnetic field aligned irregularities. Phys. Plasmas 32 (1), 012103. https://doi.org/10.1063/5.0225399, arXiv:https://pubs.aip.org/aip/pop/article-pdf/doi/10.1063/5.0225399/20337212/012103_1_5.0225399.pdf.

Ganguli, G., Crabtree, C., Fletcher, A., et al., 2025. Orbital debris-generated ion acoustic solitons in isothermal magnetized plasma. Phys. Plasmas 32 (2), 022902. https://doi.org/10.1063/5.0238686, arXiv:https://pubs.aip.org/aip/pop/article-pdf/doi/10.1063/5.0238686/20385925/022902_1_5.0238686.pdf.

Jaiswal, S., Bandyopadhyay, P., Sen, A., 2016. Experimental observation of precursor solitons in a flowing complex plasma. Phys. Rev. E 93. https://doi.org/10.1103/PhysRevE.93.041201.

Kasahara, Y., Kasaba, Y., Kojima, H., et al., 2018. The plasma wave experiment (pwe) on board the arase (erg) satellite. Earth, Planets and Space 70 (1). https://doi.org/10.1186/s40623-018-0842-4.

Kasahara, Y., Kojima, H., Matsuda, S. et al., 2021. The pwe/ofa instrument level-3 wave property data of exploration of energization and radiation in geospace (erg) arase satellite. doi:10.34515/DATA.ERG-08003.

Kumamoto, A., Tsuchiya, F., Kasahara, Y., et al., 2018. High frequency analyzer (hfa) of plasma wave experiment (pwe) onboard the arase spacecraft. Earth, Planets and Space 70. https://doi.org/10.1186/s40623-018-0854-0.

Malaspina, D.M., Tigik, S.F., Vaivads, A., 2022. Evidence that interaction with the spacecraft plasma wake generates plasma waves close to the electron cyclotron frequency in the near-sun solar wind. Astrophys. J. Lett. 936. https://doi.org/10.3847/2041-8213/ac8c8f.

Matsuda, S., Kasahara, Y., Kojima, H., et al., 2018. Onboard software of plasma wave experiment aboard arase: instrument management and signal processing of waveform capture/onboard frequency analyzer. Earth, Planets and Space 70. https://doi.org/10.1186/s40623-018-0838-0.

Matsuoka, A., Teramoto, M., Nomura, R., et al., 2018. The arase (erg) magnetic field investigation. Earth, Planets and Space 70. https://doi.org/10.1186/s40623-018-0800-1.

Miyoshi, Y., Shinohara, I., Jun, C.-W., 2018. The level-2 orbit data of exploration of energization and radiation in geospace (erg) arase satellite. doi:10.34515/DATA.ERG-12000.

Miyoshi Y, S.I., Takashima T, A.K., Higashio N, M.T. et al., 2018. Geospace exploration project erg. Earth, Planets and Space, 70(101). https://doi.org/10.1186/s40623-018-0862-0.

Mukherjee, A., Acharya, S.P., Janaki, M.S., 2021. Dynamical study of nonlinear ion acoustic waves in presence of charged space debris at low earth orbital (leo) plasma region. Astrophys. Space Sci. 366. https://doi.org/10.1007/s10509-020-03914-2.

Resendiz Lira, P.A., Delzanno, G.L., Svyatsky, D. et al., 2024. On ion-acoustic precursor soliton signatures of orbital debris in low earth orbit. J. Spacecr. Rock., 61(6), 1640–1655. URL: doi: 10.2514/1.A35985. doi:10.2514/1.A35985. arXiv:https://doi.org/10.2514/1.A35985.

Sen, A., Mukherjee, R., Yadav, S.K., et al., 2023. Electromagnetic pinned solitons for space debris detection. Phys. Plasmas 30. https://doi.org/10.1063/5.0099201.

Sen, A., Tiwari, S., Mishra, S., et al., 2015a. Nonlinear wave excitations by orbiting charged space debris objects. Adv. Space Res. 56 (3).

Sen, A., Tiwari, S., Mishra, S., et al., 2015b. Nonlinear wave excitations by orbiting charged space debris objects. Adv. Space Res. 56. https://doi.org/10.1016/j.asr.2015.03.021.

Tiwari, S.K., Sen, A., 2016a. Fore-wake excitations from moving charged objects in a complex plasma. Phys. Plasmas 23. https://doi.org/10.1063/1.4964908.

Tiwari, S.K., Sen, A., 2016b. Wakes and precursor soliton excitations by a moving charged object in a plasma. Phys. Plasmas 23. https://doi.org/10.1063/1.4941092.

Truitt, A., Hartzell, C., 2020a. Simulating plasma solitons from orbital debris using the forced korteweg–de vries equation. J. Spacecr. Rock. 57 (5). https://doi.org/10.2514/1.A34652.

Truitt, A., Hartzell, C., 2020b. Three-dimensional kadomtsev–petviashvili damped forced ion acoustic solitary waves from orbital debris. J. Spacecr. Rock. 58 (3). https://doi.org/10.2514/1.A34805.

Truitt, A.S., Hartzell, C.M., 2020c. Simulating damped ion acoustic solitary waves from orbital debris. J. Spacecr. Rock. 57. https://doi.org/10.2514/1.A34674.

Truitt, A.S., Hartzell, C.M., 2020d. Simulating plasma solitons from orbital debris using the forced korteweg–de vries equation. J. Spacecr. Rock. 57. https://doi.org/10.2514/1.A34652.

Truitt, A.S., Hartzell, C.M., 2021. Three-dimensional kadomtsev–petviashvili damped forced ion acoustic solitary waves from orbital debris. J. Spacecr. Rock. 58, 848–855. https://doi.org/10.2514/1.A34805.